# Hall A Status

## Overview of topics

- Hall A schedule update
- GEp

# Upcoming Hall A schedule

- March 20 beams ends for GEn
- March 20-May 20th
  - Rent crane from Barnhardt to change over from GEn to GEn-RP
  - Remove polarized target.
  - Install scattering chamber, position SBS/BB/HCAL
  - SBS rear clamp, SBS lead wall, Side GEM/hodo planes, SBS GEM work?
- May 20th-July20th
  - Hall A ceiling crane repair work
- July 20th - Aug20th
  - Install cryotarget (one for GEn-RP and GEp combined),
  - cool down and prepare Hall
- Aug 20th - Sept 20th
  - Run GEn-RP at 4.3  (5 PAC days prod. 5 PAC days commissioning)
  - Run K_LL , 2 PAC days at 4.3 (calib Ay), 2 PAC at 6.4 (prod) ,( if targets with radiator can be installed)
- Sept 20th 2023 - July 20th 2024
  - Deinstall BigBite detector and electronics
  - Install ECAL & CDET detectors and electronics, rearrange GEM chambers into GEp SBS frame
- July 20th 2024 - Oct 20th 2024
  - Run GEp

# Elastic ep scattering

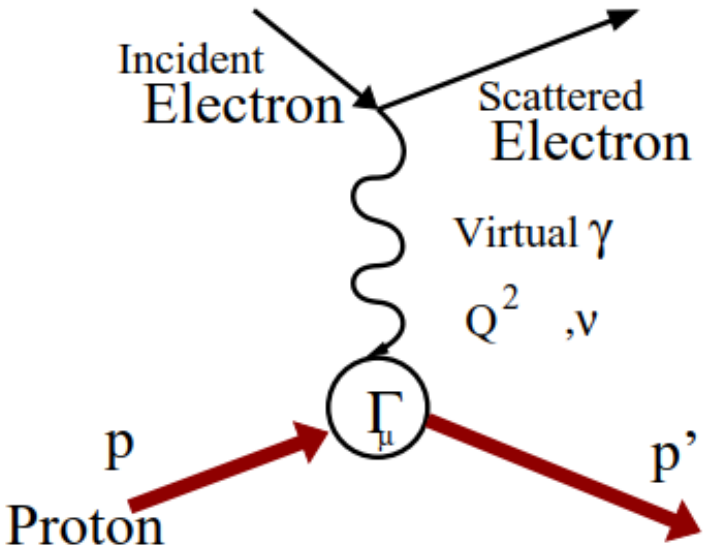


Nucleon vertex:

$$\Gamma_\mu(p',p) = \underbrace{F_1(Q^2)}_{Dirac}\gamma_\mu + \frac{i\kappa_p}{2M_p}\underbrace{F_2(Q^2)}_{Pauli}\sigma_{\mu\nu}q^\nu$$

$$G_E(Q^2) = F_1(Q^2) - \kappa_N \tau F_2(Q^2)$$

$$G_M(Q^2) = F_1(Q^2) + \kappa_N F_2(Q^2), \tau = \frac{Q^2}{4M_N}$$

At $Q^2 = 0$ $\quad G_{Mp} = 2.79\ G_{Mn} = -1.91$

$$G_{Ep} = 1\ G_{En} = 0$$

Extract $G_E$ and $G_M$ from:

- Cross-section measurements $N(e,e')$
- Beam-target Asymmetries $\vec{N}(\vec{e},e')N$
- Recoil polarization $N(\vec{e},e')\vec{N}$

# GMp and two photon effects in electron-proton scattering

Results published March 11, 2022 in Phys. Rev. Lett. 102002

$$\sigma_R = \tau\, G_M^2(Q^2) + \varepsilon\, G_E^2(Q^2) = \sigma_T + \varepsilon\, \sigma_L$$
$$= G_M^2(Q^2)(\tau + \varepsilon\, \mathrm{RS}(Q^2)/\mu_p^2),$$
$$G_M = \mu_p(1 + a_1\tau)/(1 + b_1\tau + b_2\tau^2 + b_3\tau^3),$$
$$\mathrm{RS} = 1 + c_1\tau + c_2\tau^2.$$

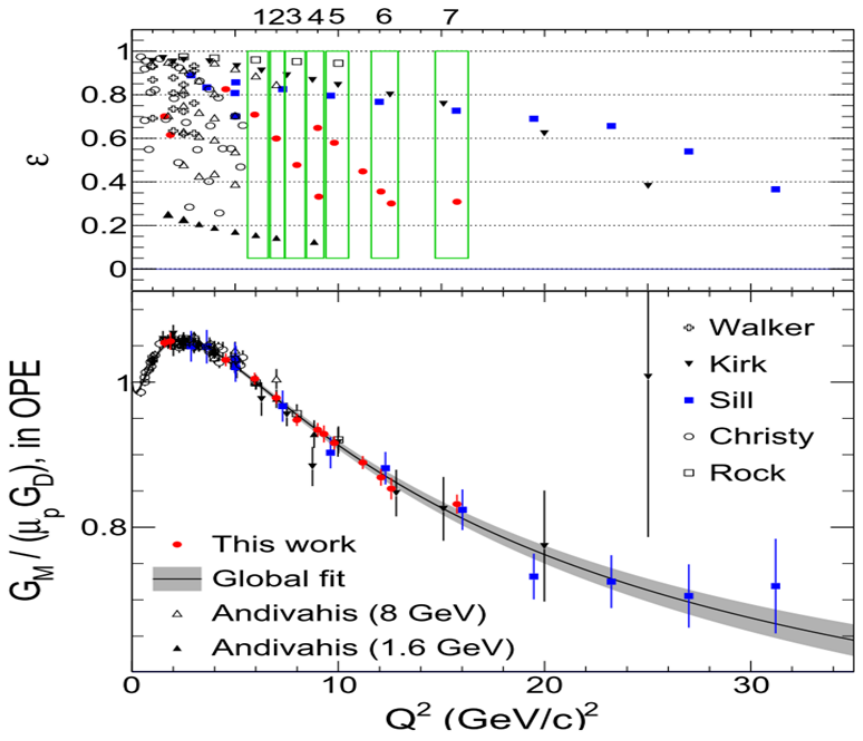


FIG. 1. (Top) Kinematics of elastic $e$-$p$ cross section data used in the global fit and Rosenbluth separations; the boxes (1-7) indicate the groupings of points for the Rosenbluth separations. (Bottom) The effective proton magnetic form factor, normalized by the standard dipole $\mu_p G_D$, obtained from the cross section measurements of GMp12 and Refs. [4–6, 20, 35, 39], with symbols as indicated in the plot's legend. The curve shows the result of our global fit, with the gray shaded area indicating the 68% confidence interval.

**Global fit to Sill, Andivahis, Christy, and GMp12, all with updated RC, plus direct LT separation points (do not reflect the full high $Q^2$ data set)**

Minimal low-$Q^2$ data included: fit focused on high-$Q^2$ behavior

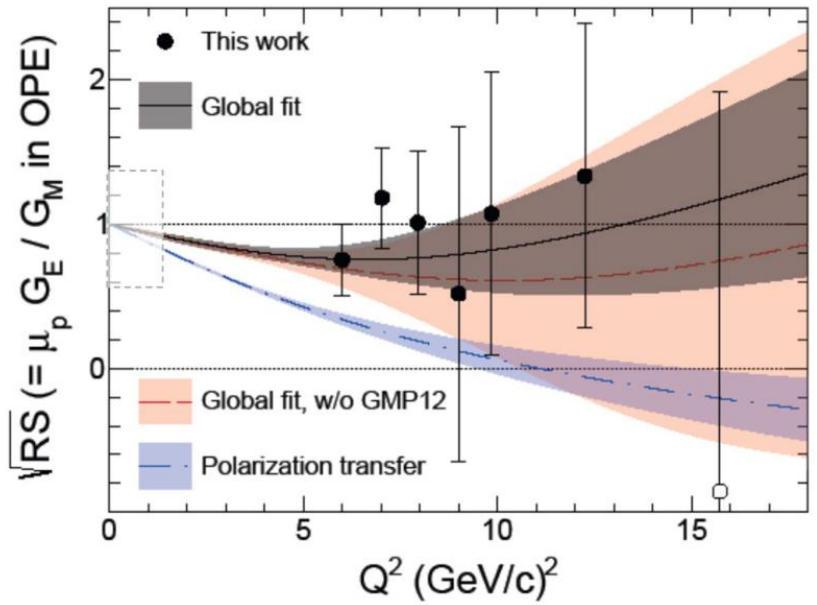


**New data, updated RC: $\langle\Delta_{2\gamma}\rangle$ = 4.2 ± 2.0% (for $Q^2$>6 GeV$^2$)**

**Indications of TPE over full $Q^2$ range**



Jefferson Lab

# GEp experiment

| $Q^2$ | $E_{beam}$ | $\theta_e$ | $\theta_p$ |
|---|---|---|---|
| 5.7 | 6.4 | 29.8 | 25.7 |
| 8.1 | 8.5 | 27.5 | 22.1 |
| 12.0 | 10.6 | 30.0 | 16.7 |

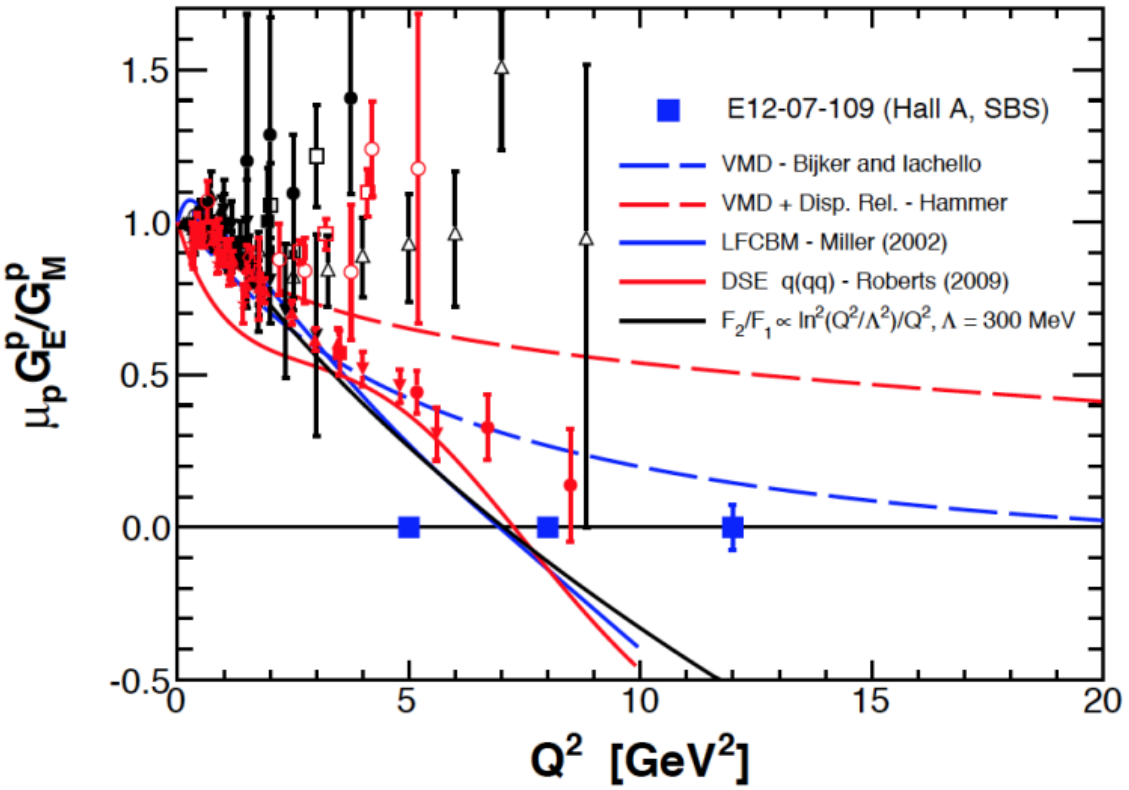


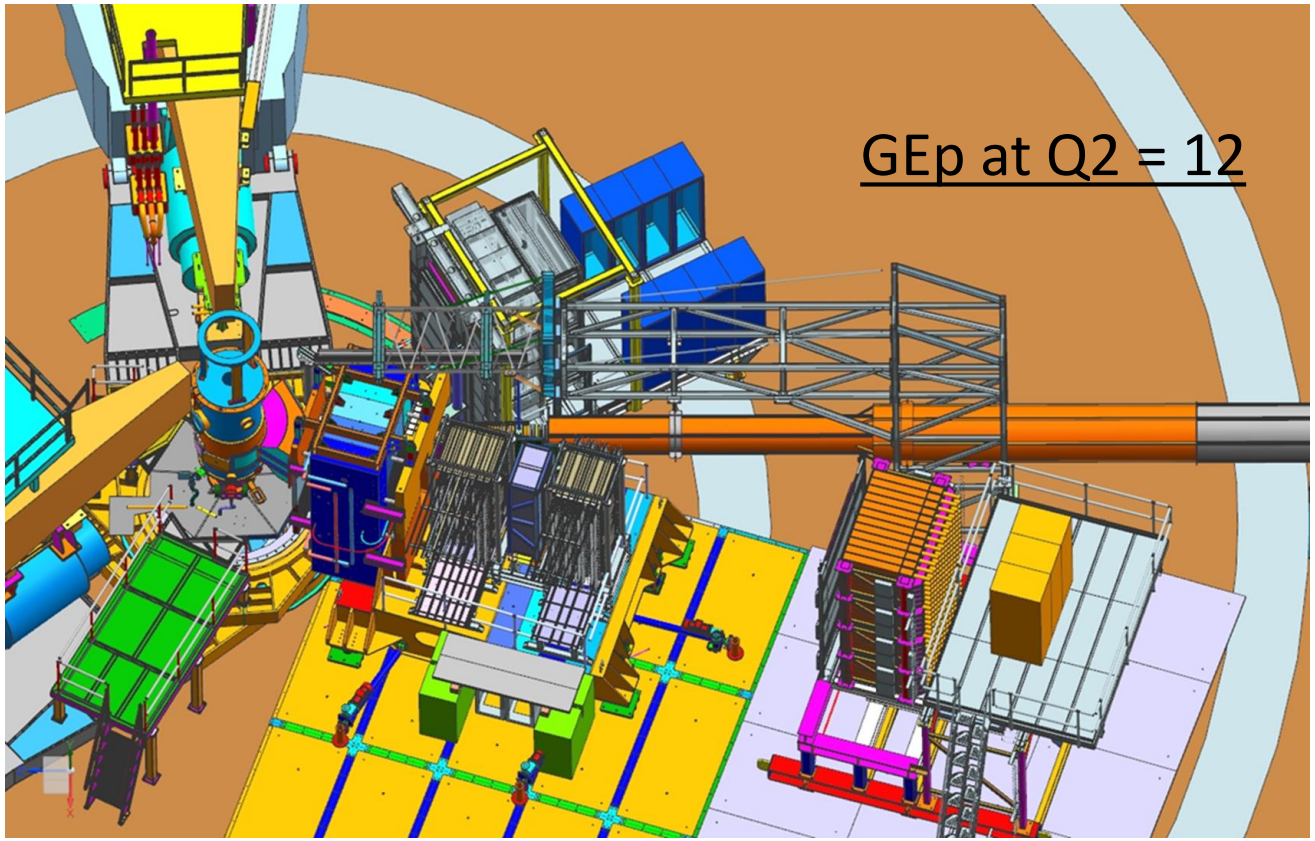


Polarimeter is 8 chambers in front, 50cm of CH, 8 chamber in rear.
Use HCAL as part of coincidence trigger.

# Relationship between $G_E/G_M$ and observables

$$\chi_\theta = \gamma(\mu_p - 1)(\theta_B + \theta - \theta^{fp})$$

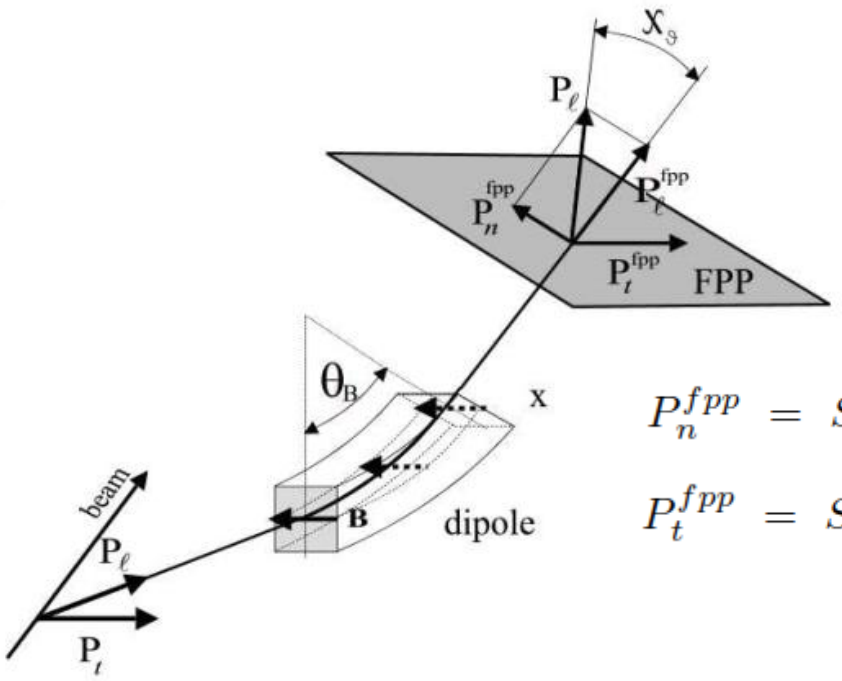


$$P_n^{fpp} = S_{nt} h P_t + S_{n\ell} h P_\ell$$

$$P_t^{fpp} = S_{tt} h P_t + S_{t\ell} h P_\ell$$

$$P_t^{fpp} = hP_t \text{ and } P_n^{fpp} = hP_\ell \sin\chi_\theta.$$

$$P_t = -hP_e\sqrt{\frac{2\epsilon(1-\epsilon)}{\tau}}\frac{r}{1+\frac{\epsilon}{\tau}r^2} \qquad \tau \equiv Q^2/4M_p^2$$

$$P_\ell = hP_e\frac{\sqrt{1-\epsilon^2}}{1+\frac{\epsilon}{\tau}r^2} \qquad \epsilon \equiv \left[1+2(1+\tau)\tan^2(\theta_e/2)\right]^{-1}$$

$$r \equiv \frac{G_E^p}{G_M^p} = -\frac{P_t}{P_\ell}\sqrt{\frac{\tau(1+\epsilon)}{2\epsilon}} = \frac{R}{\mu_p},$$

$P_l$ is about 0.7 for the GEp kinematics. Insensitive to R

$P_t$ is sensitive to R

# Determining the focal plane asymmetries

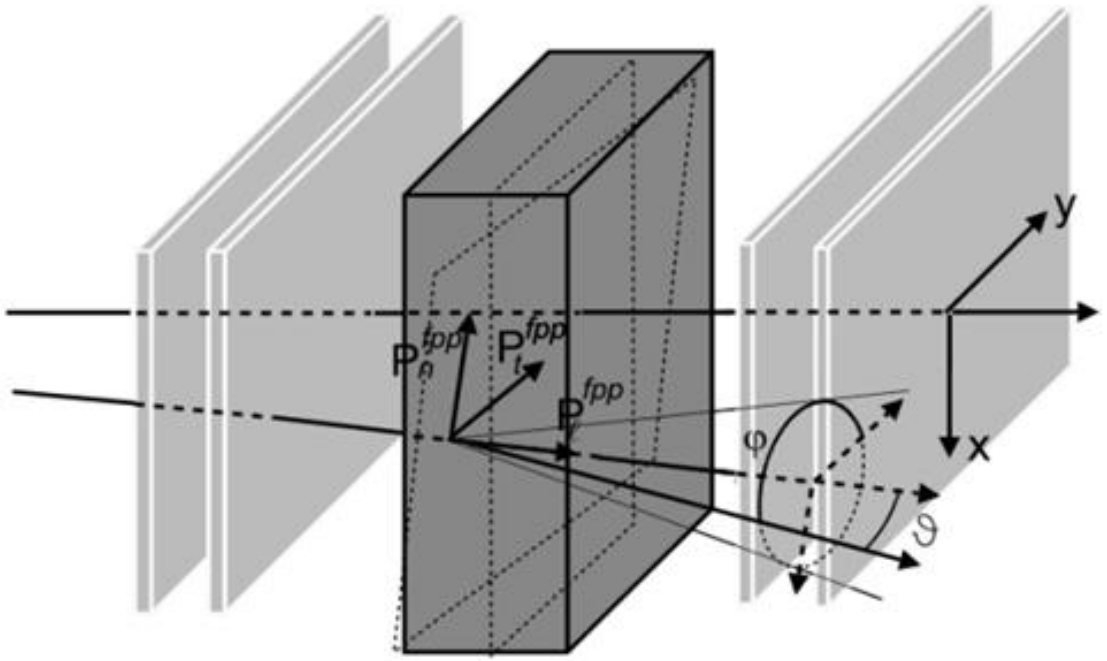


FIG. 9. Principle of the polarimeter, showing a noncentral trajectory through the front chambers, scattering in the analyzer, and a track through the back chambers; $\vartheta$ is the polar angle, and $\varphi$ is the azimuthal angle from the $y$ direction counterclockwise.

$$N^{\pm}(p,\vartheta,\varphi) = N_0^{\pm}\frac{\varepsilon(p,\vartheta)}{2\pi}\left[1 + (\pm A_y P_x^{FPP} + c_1)\cos\varphi + (\mp A_y P_y^{FPP} + s_1)\sin\varphi + c_2\cos(2\varphi) + s_2\sin(2\varphi) + \ldots\right]$$

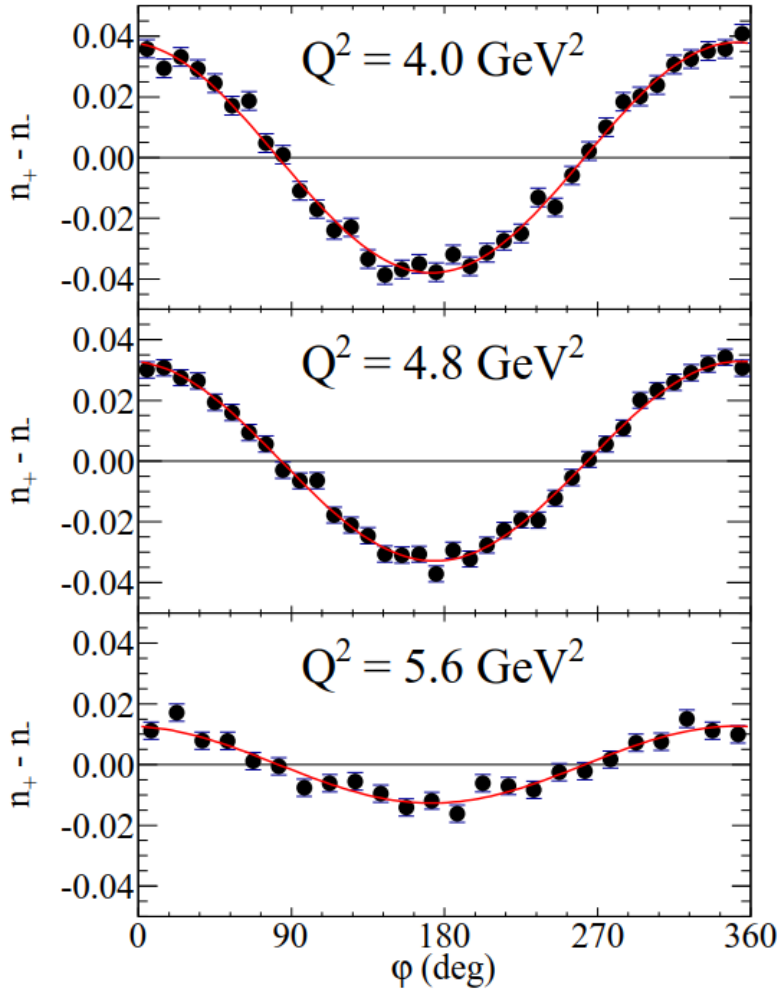


$$n_+ - n_- \equiv (N_{bins}/2)\left[N^+(\varphi)/N_0^+ - N^-(\varphi)/N_0^-\right]$$

A.P.J. Puckett et al Phys. Rev. C 85:045203 (2012)

# Poincare-covariant quark+diquark Faddeev calculation

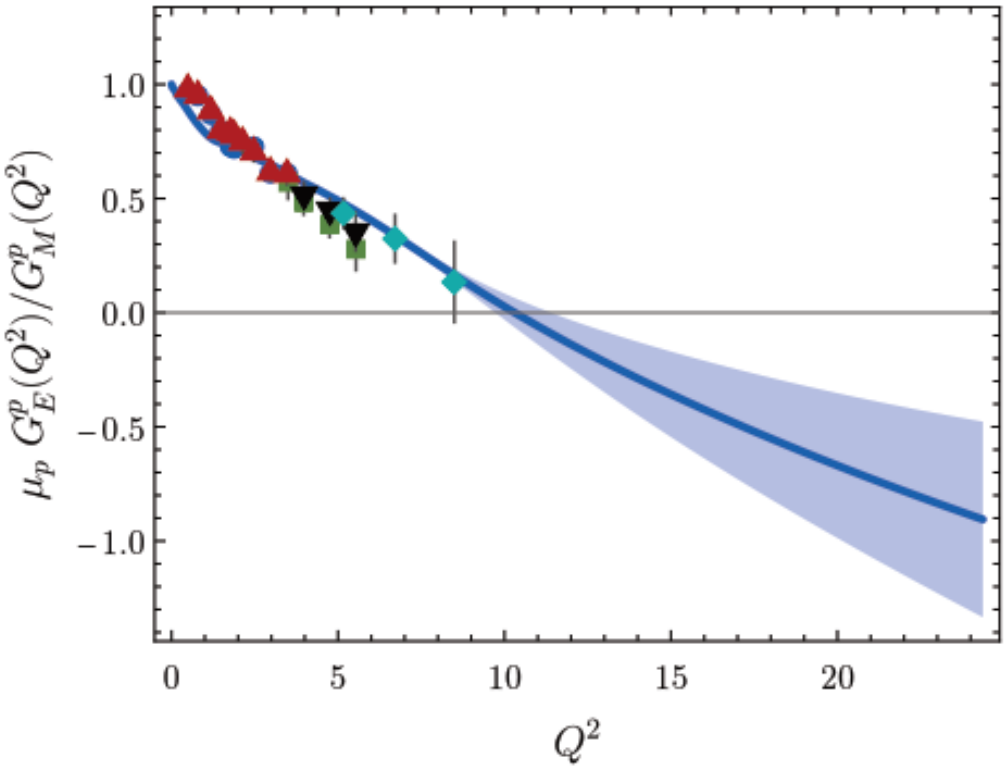


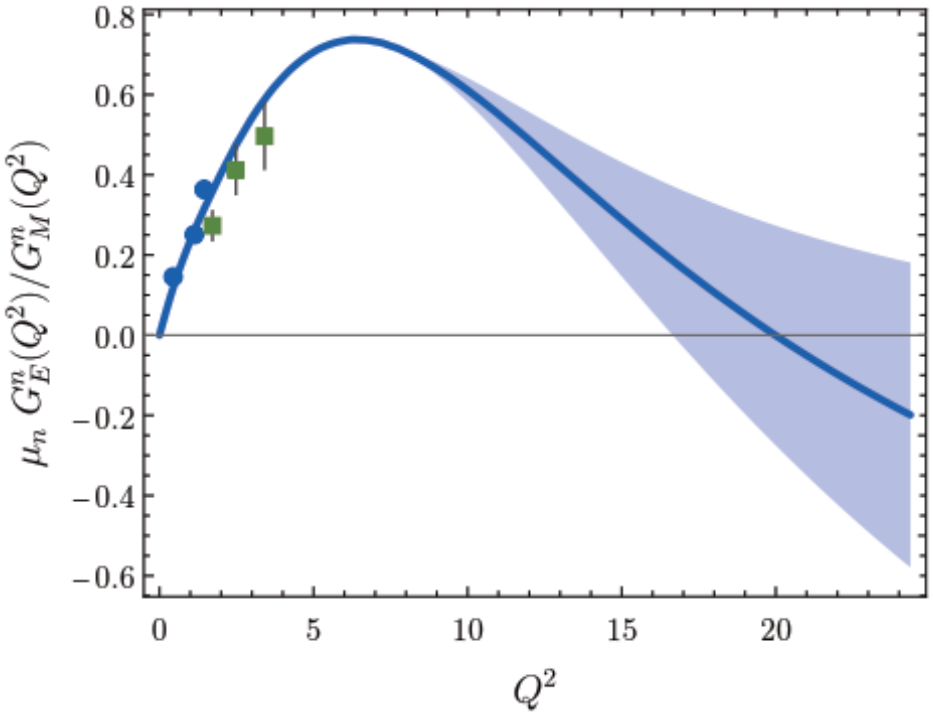


Previous paper in 2013 had zero crossing at $Q^2 = 12$
This paper improves

Zhu-Fang Cui,[1,2,*] Chen Chen,[3,†] Daniele Binosi,[4,‡] Feliciano De Soto,[5,§] Craig D. Roberts,[1,2,¶]
José Rodríguez-Quintero,[6,**] Sebastian M. Schmidt,[7,8,††] and Jorge Segovia[9,2,‡‡]

Phys. Rev. D 102, 014043 (2020)

# Comparison quark $F_1$ and $F_2$

$$F_i^u = 2F_i^p + F_i^n,\ F_i^d = F_i^p + 2F_i^n\ , i = 1, 2$$

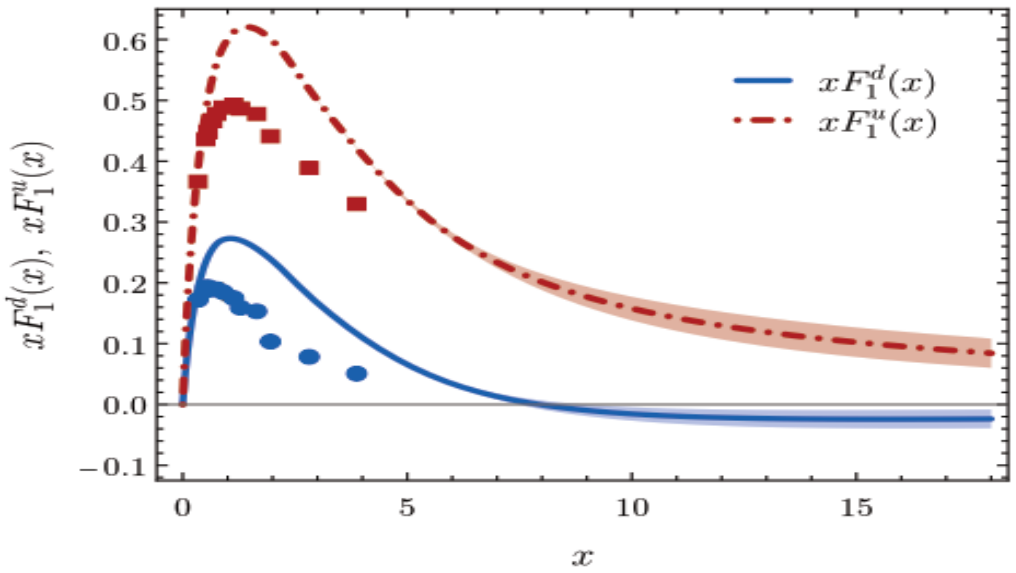


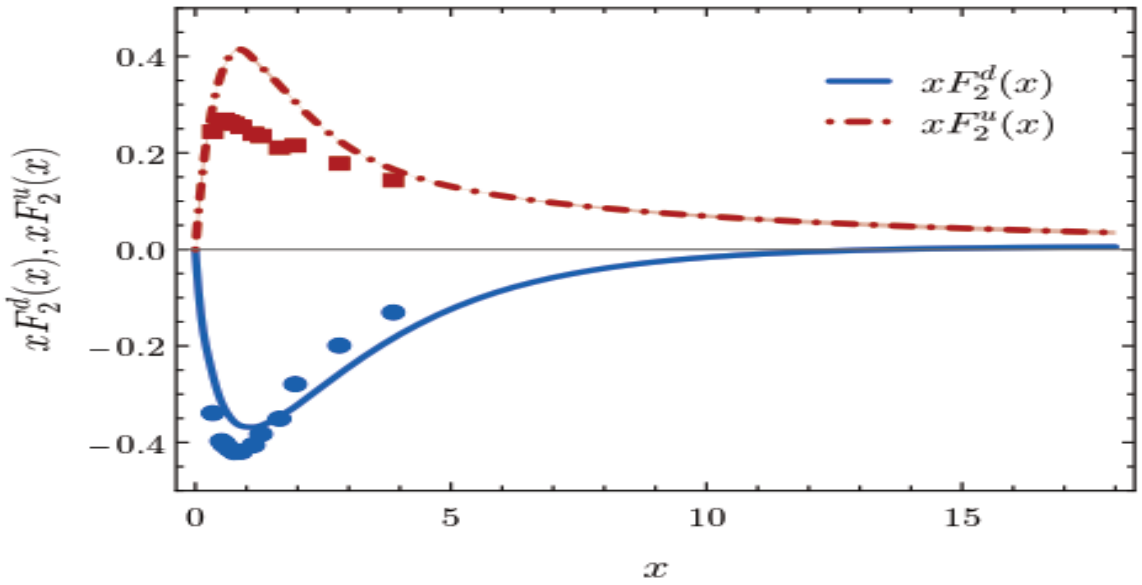


- The ud diquark dominates the Faddeev wave-function
- F1u larger than F1d indicates that ep scattering dominated by u-quark that is not in the ud diquark
- Smaller pseudovector diquark component exist .
  - Zero in F1d indicates relative probability of finding  scalar and pseudovector diquarks in proton

# Data Comparison to Lattice QCD calculations

C. Kallidonis *et al.*, PoS **LATTICE2018**, 125 (2018).

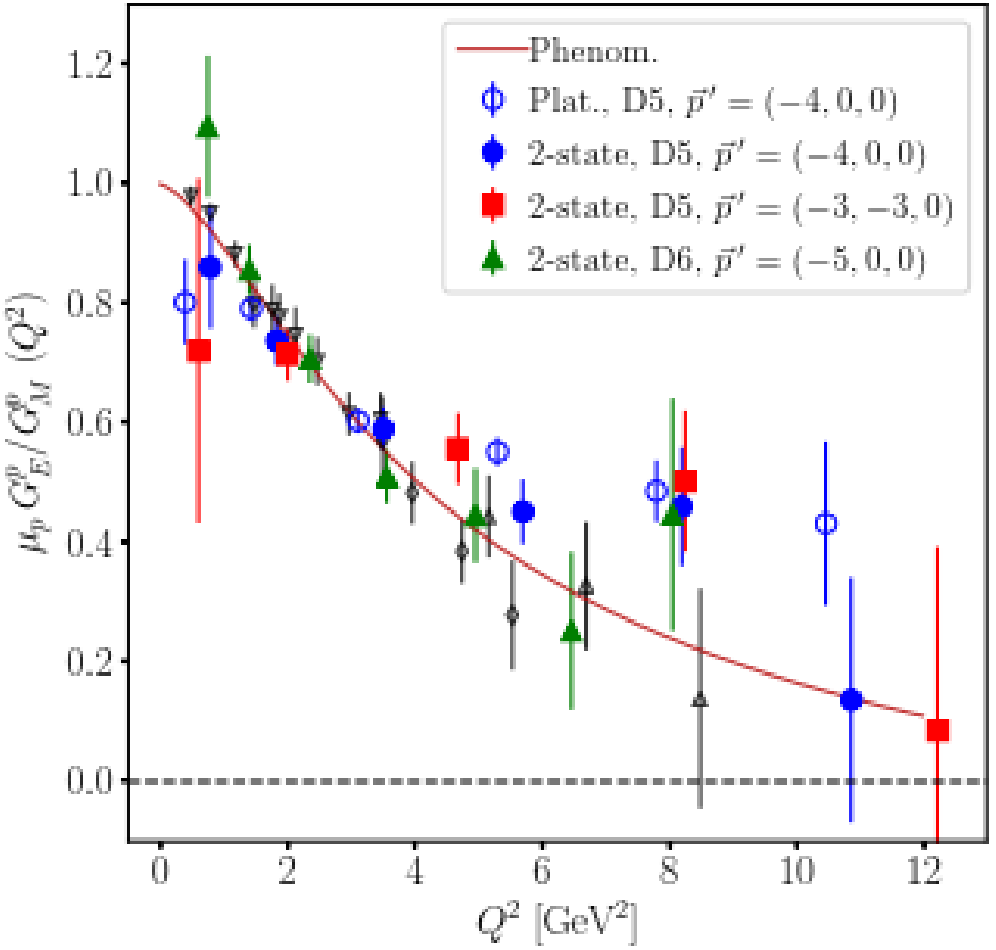


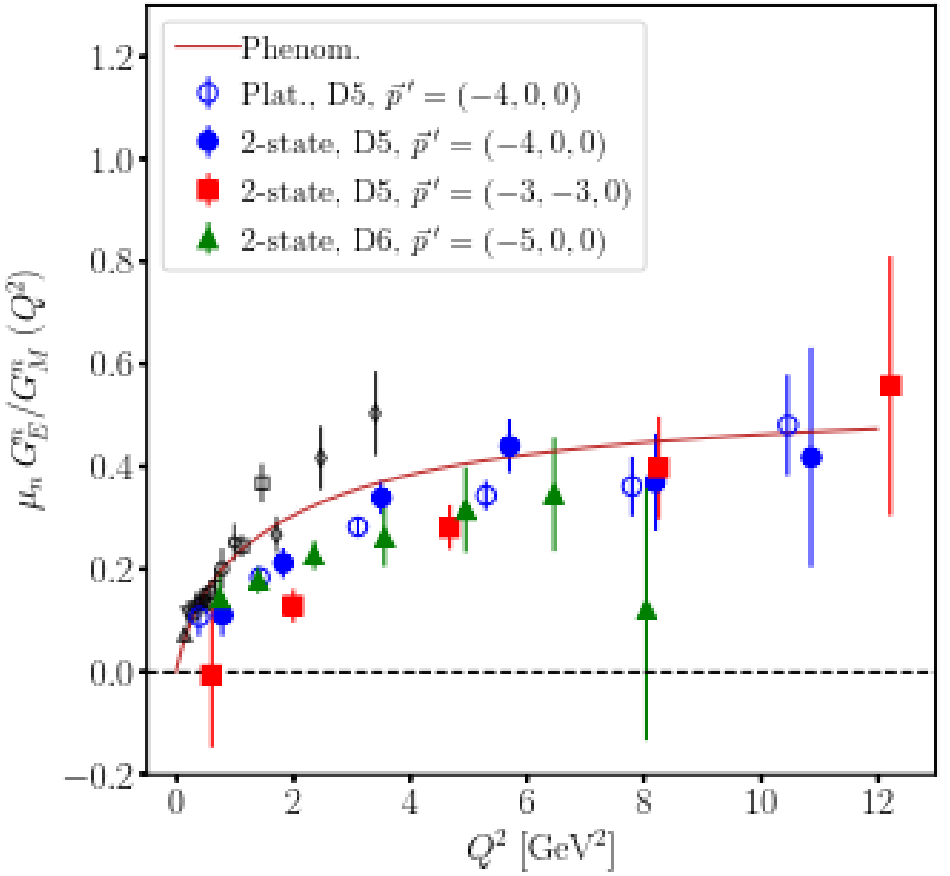


Disconnected diagrams not included.
May explain the smaller GEn/GMn from lattice